Electronic Supplementary Material (ESI) for Nanoscale.
This journal is © The Royal Society of Chemistry 2017

Boosting Efficiency of Inverted Quantum Dot Light-Emitting Diodes by Balancing Charge Densities and Suppressing Exciton Quenching Through Band Alignment

Jiangyong Pan, [a,†] Changting Wei, [b, †] Lixi Wang, [a] Jinyong Zhuang, [b] Qianqian Huang, [a] Wenming Su,[b,*] Zheng Cui, [b] Arokia Nathan, [c] Wei Lei [a, *] Jing Chen [a, *]

[a]Joint International Research Laboratory of Information Display and Visualization, School of Electronic Science and Engineering, Southeast University, Nanjing, 210096, China

[b] Printable Electronics Research Centre, Suzhou Institute of Nano-Tech and Nano-Bionics (SINANO), Chinese Academy of Sciences, Suzhou 215123, China

[c] Electrical Engineering Division, Engineering Department, University of Cambridge, 9 JJ Thomson Avenue, CB3 0FA, Cambridge, United Kingdom

SI-1 The valence band maximum (VBM) of QDs was estimated by using incident photon energy (21.2 eV), the high-binding energy cutoff (Ecutoff) (Figure S1(a)), and the onset energy in valence-band region (Eonset) (Figure S1(b)) according to the equation of VBM = 21.2 − (Ecutoff − Eonset). Thus the VBM of QDs were deduced of 7.1 eV. Based on the band gap values required from the absorption spectra of QDs (Figure 1 in the manuscript), the CBM levels were estimated to be 4.8 eV.

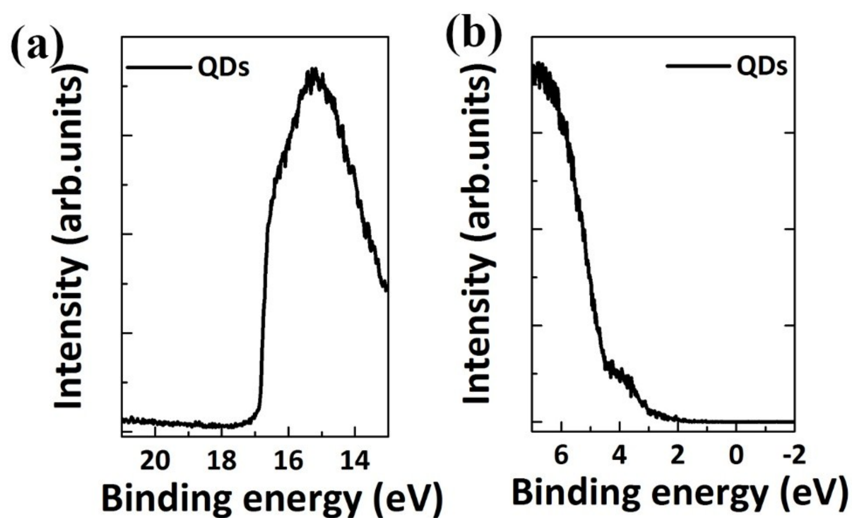

Figure S1 UPS spectra showing (a) high-binding energy secondary electron cutoff and (b) valence-band edge regions of QD solid films

SI-2 It is displayed in the Figures S2(a) that the ZnO NPs have the average diameter of about 3 nm. The absorption and photoluminescence spectra of the ZnO NPs are shown in Figure S2(b). It is observed that the peak position of absorption is located at 347 nm. The band gap Eg of the colloidal ZnO NPs is determined from the intercept between the wavelength axis and the tangent to the linear section of the absorption band edge. The band gap is 3.46 eV for the ZnO NPs, which is higher than that of bulk ZnO (3.2–3.3 eV), indicating that there is a higher spatial confinement of photo-generated charge carriers in the smaller ZnO particles. It can be seen from Figure S2(c) that our synthesized ZnO NPs have a wurtzite structure, which is in good agreement with the literature values (JCPDS card no. 79-0207), although the small particle size led to a significant broadening of the characteristic diffraction pattern. The electron mobility of the ZnO film is obtained as shown in Figure S2(d) by fitting space-charge-limited-current region ($J \propto V^2$) with Child's law, $J = \left(\frac{9}{8}\right)\varepsilon_r \varepsilon_0 \mu_e V^2/d^3$, where ε_0, ε_r, μ_e and d are the vacuum permittivity, relative permittivity, electron mobility and film thickness, respectively. By assuming that ε_r=4, μ_e is determined to be 1.0×10^{-3} $cm^2\ V^{-1}\ s^{-1}$.

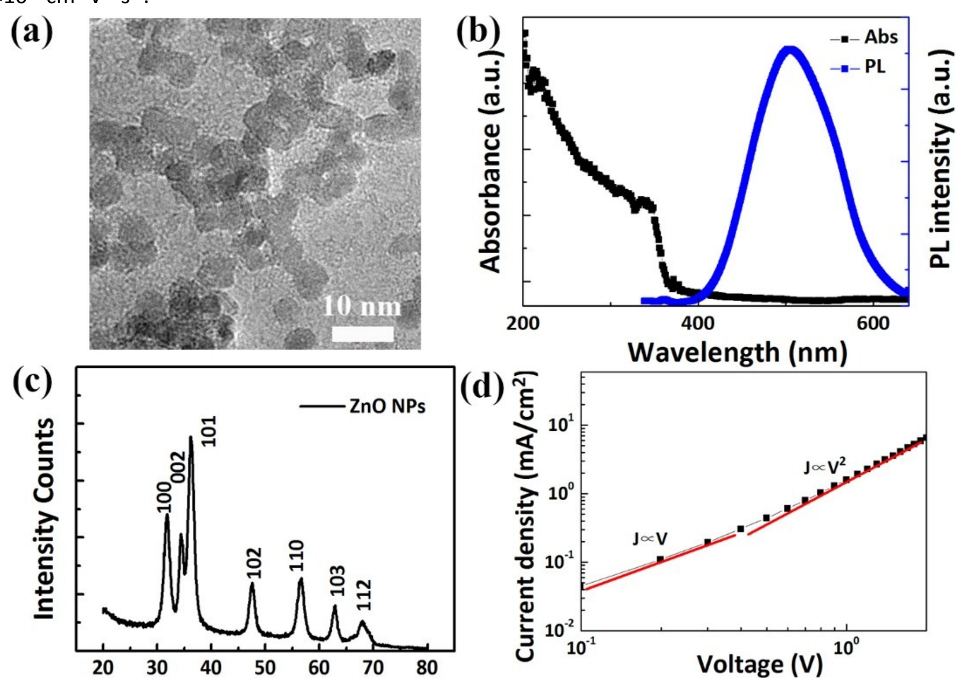

Figure S2 (a) TEM image of ZnO NPs, (b) absorption and photoluminescence spectra of ZnO NPs, (c) XRD pattern from ZnO NPs film, (d) Current density–voltage (J–V) characteristics of an electron-only device (ITO/Al/ZnO/Al).

SI-3 The XPS spectra of ZnO:CsN_3 films is displayed in the Figure S3. The asymmetric O1s peaks of ZnO:CsN_3 are thoroughly de-convoluted into three Gaussian distributions, which are centered at 530.0±0.1 eV (OI), 531.1±0.1 eV (OII) and 532.0±0.1 eV (OIII), respectively

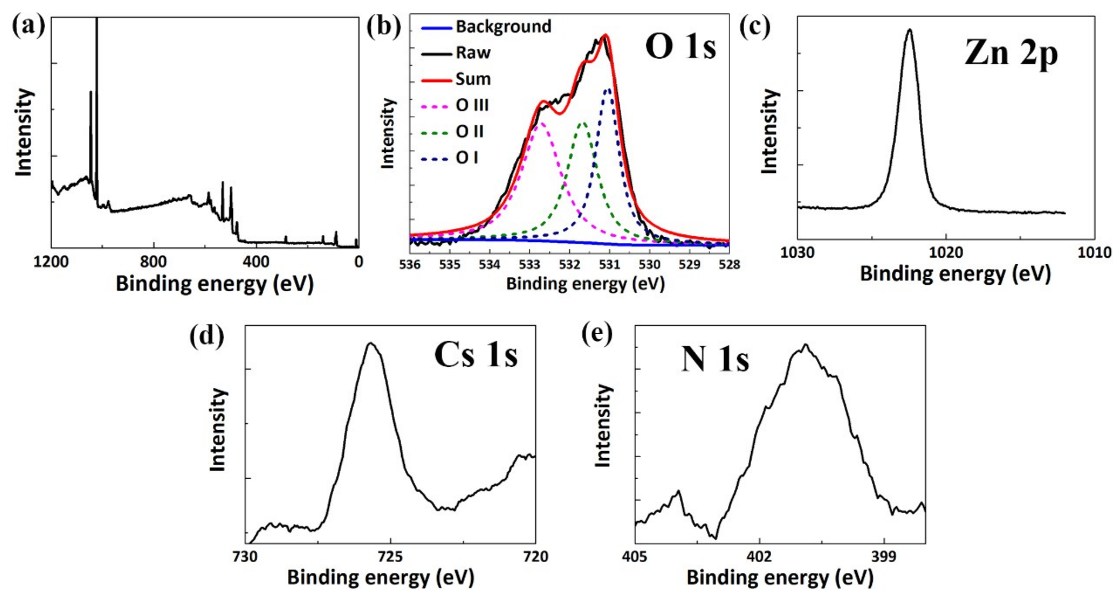

Figure S3 (a) XPS spectra of ZnO:CsN_3 films. Binding energy of the (b) O 1s core level , (c) Zn 2p core level, (d) Cs 1s core level and (e) N 1s core level for ZnO layer surface

SI-4 The electronic structure of the doped ZnO NP films with different doping concentration were investigated by ultraviolet photoelectron spectroscopy (UPS) measurements. The resulting secondary-electron cutoff and valence band regions are shown in Figure S4a and b, respectively. Generally, the work function (WF) could be estimated by the difference between the incident light energy (21.2 eV) and the energy of secondary cutoff. In this case, the WF of ZnO and ZnO doped with different concentration of CsN_3 are calculated and labeled in Figure S4a. In order to define the position of the valence band maximum (VBM), the energy gap between Fermi level and VBM (ΔE_{VB}) is extracted from the valence-band region and labeled in Figure S4b. As a result, via the summation of WF and ΔE_{VB}, the VBM levels of ZnO and ZnO doped with different concentration of CsN_3 are calculated and summarized in Table S1. Figure S4d shows the absorption spectra of ZnO and ZnO:CsN_3, based on data converted from Figure S4c. The band gaps (Eg) of these materials could be determined through the absorption onset of the linear region and the Eg values are labeled in the Figure S4d. Therefore, the conduction band minimum (CBM) levels of ZnO and ZnO doped with different concentration of CsN_3 are summarized in Table S1. It can be found that the CBM level decreases from 4.21 eV to 3.80 eV with increasing the doping concentration of CsN_3 in ZnO. Correspondingly, the transport barrier for electrons from cathode to ETL increases from 0.39 eV to 0.80 eV as the doping concentration of CsN_3 in ZnO increases, leading to more efficient electrons blocking. In addition, the lowering of CBM of ZnO:CsN_3 helps reduce exciton dissociation, thus reducing the exciton quenching due to the larger energy barrier between the CBM of QDs and ZnO NPs. However, the valence band maximum (VBM) of ETL shifts from 7.67 eV to 7.40 eV with increasing the doping concentration of CsN_3. The upshift of VBM can facilitate the leakage of holes and decrease the recombination efficiency of exciton in the emissive layer. Therefore the doping concentration of CsN_3 will be optimized according to the carrier only devices and performance of QLEDs demonstrated in the manuscript.

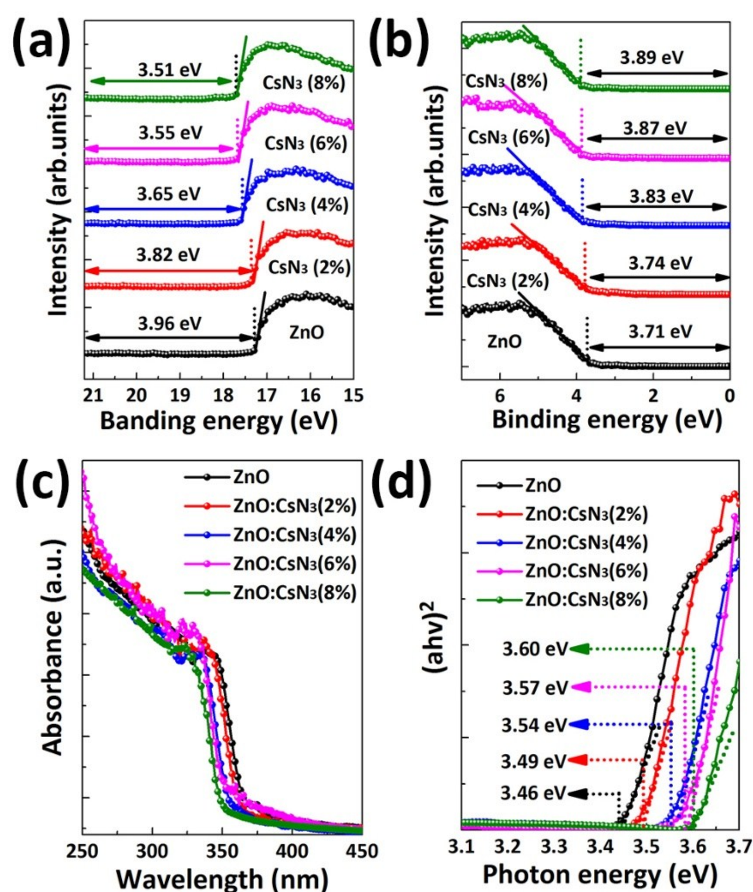

Figure S4 UPS spectra showing (a) high-binding energy secondary electron cutoff and (b) valence-band edge regions

of ZnO and ZnO doped CsN_3 films (doping ratio is 2, 4, 6, 8 vol%, respectively). (c) Absorption spectra of ZnO, (d) $(Ahv)^2$–hv plots converted from (c)

Table S1. Summary of valence band maximum (VBM), band gaps (Eg) and conduction band minimum (CBM) levels of ZnO and ZnO doped with different doping concentrations of CsN_3

	ZnO	$ZnO:CsN_3$ (2 vol%)	$ZnO:CsN_3$ (4 vol%)	$ZnO:CsN_3$ (6 vol%)	$ZnO:CsN_3$ (8 vol%)
VBM (eV)	7.67	7.56	7.48	7.42	7.40
Eg (eV)	3.46	3.49	3.54	3.57	3.60
CBM (eV)	4.21	4.07	3.94	3.85	3.80

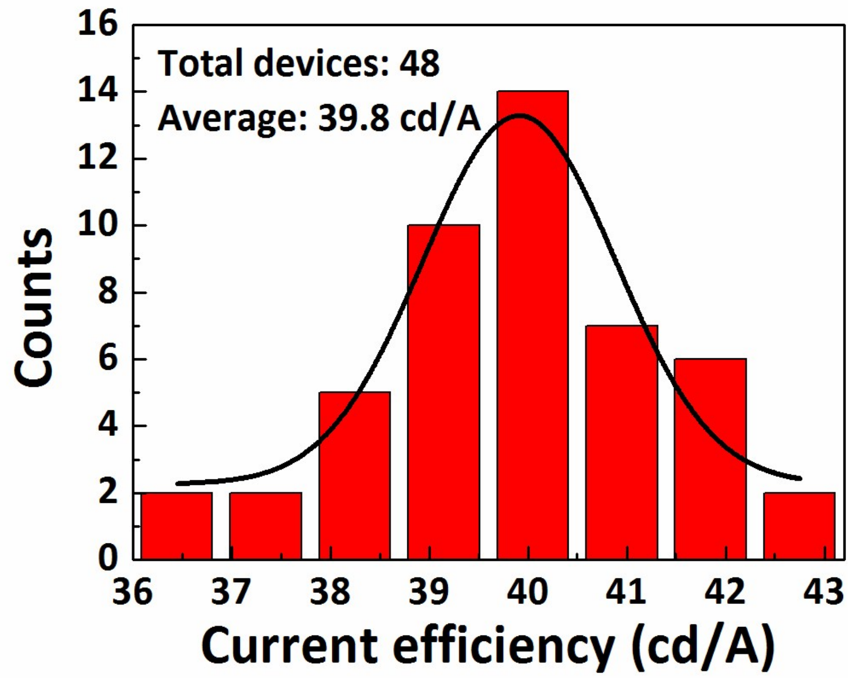

Figure S5. Histogram of current efficiencies (η_A) of 48 devices for green QLEDs. The average current efficiency is 39.8 cd/A.

SI-5 It is noted that the PL decay of QDs on glass substrate is determined by intrinsic recombination in QDs. Thus, it can be well fitted with a bi-exponential decay model[1],

$$I(t) = a_1 \exp(\frac{-t}{\tau_r}) + a_2 \exp(\frac{-t}{\tau_{nr}}) \quad (1)$$

where and τ_r and τ_{nr} represented radiative and nonradiative decay for QDs. However, in the case of QDs that deposited on ETL, the presence of the electron transport materials provided an additional pathway, which favors the infection of the photoexcited charge carriers. Thus, it can be well fitted with a tri- exponential decay model,

$$I(t) = a_1 \exp(\frac{-t}{\tau_r}) + a_2 \exp(\frac{-t}{\tau_{nr}}) + a_3 \exp(\frac{-t}{\tau_{ETL}}) \quad (2)$$

where and τ_r and τ_{nr} represented radiative and nonradiative decay for QDs, and . τ_{ETL} represented the interaction between QDs and ETL. The specific fitting result is summarized in Table S2.

Table S2. The best fit parameters of PL decay profiles of QD films on different ETL

	a_1 (%)	t_r (ns)	a_2 (%)	t_{nr} (ns)	a_3 (%)	t_{ETL} (ns)	$t_{av.}$ (ns)
QD	36.2	16.2	63.8	34.4			27.8
ZnO/QD	12	13.0	23	44.5	65	4.3	14.6
ZnO:CsN_3/QD	20.2	13.3	39.8	43.3	40	6.2	22.4

As discussed in the manuscript, a spontaneous charge transfer process occurs owing to the difference in work functions between ZnO and QDs, leaving positively charged QDs when the QDs were in direct contact with the ZnO ETLs, which can be evidenced by the existence of a_3 and τ_{ETL} . Meanwhile the charging of the QDs causes inefficient trion emissions,[2] as indicated by the decrease in the a_1 (from 36.2% to 12.0%)and τ_r (from 16.2 ns to 13.0 ns), which made a major contribution to the reduction of the average lifetime $\tau_{av.}$ from 27.8 ns to 14.6 ns. The doping of ETL by CsN_3 modifies the QD/ZnO interface, thus decreases the fraction of a_3 from 65% to 40%. This can be attributed to the larger energy barrier (0.86 eV) for exciton dissociation between the CB of QDs and ZnO NPs after doping of 4% CsN_3 in the ZnO as indicated in Figure 3 in the manuscript and Figure S4, and the inhibition effect of the insulating layer on exciton quenching induced by ZnO nanoparticles. Further, it can increase the average lifetime $\tau_{av.}$ from 14.6 ns to 22.4 ns.

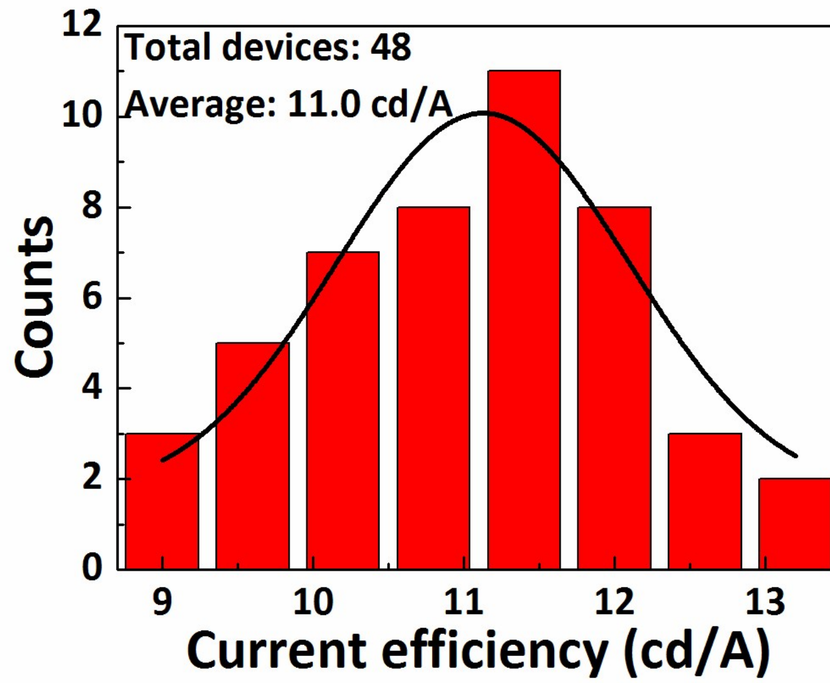

Figure S6. Histogram of current efficiencies (η_A) of 48 devices for red QLEDs. The average current efficiency is 11.0 cd/A.

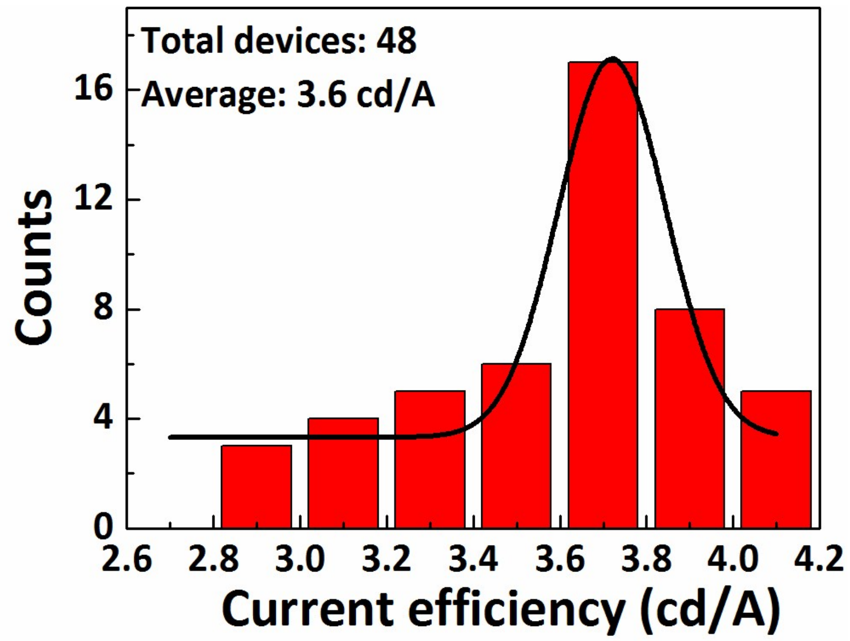

Figure S7. Histogram of current efficiencies (η_A) of 48 devices for blue QLEDs. The average current efficiency is 3.6 cd/A.

References

1. Li, J.; Xu, L.; Wang, T.; Song, J.; Chen, J.; Xue, J.; Dong, Y.; Cai, B.; Shan, Q.; Han, B.; Zeng, H., 50-Fold EQE Improvement up to 6.27% of Solution-Processed All-Inorganic Perovskite CsPbBr3 QLEDs via Surface Ligand Density Control. *Adv. Mater.* **2016,** *29* (5), 1603885-1603893.

2. JavauxC; MahlerB; DubertretB; ShabaevA; Rodina, A. V.; EfrosAl, L.; Yakovlev, D. R.; LiuF; BayerM; CampsG; BiadalaL; BuilS; QuelinX; Hermier, J. P., Thermal Activation of Non-radiative Auger Recombination in Charged Colloidal Nanocrystals. *Nat Nano* **2013,** *8* (3), 206-212.